Isogeometric Bi-Directional Evolutionary Structural Optimization

LING YIN[1], FEI ZHANG[1], XIAOWEI DENG[2,3], PENG WU[1], HONGXIN ZENG[4,5], AND MEI LIU[6]

[1]School of Mechanical Engineering, Dongguan University of Technology, Dongguan 523808, China
[2]Department of Civil Engineering, The University of Hong Kong, Hong Kong
[3]State Key Laboratory of Structural Analysis for Industrial Equipment, Dalian University of Technology, Dalian 116024, China
[4]School of Economics and Management, Dongguan University of Technology, Dongguan 523808, China
[5]Hunan Provincial Key Laboratory of Health Maintenance for Mechanical Equipment, Xiangtan 411201, China
[6]School of Automation, Guangdong University of Petrochemical Technology, Maoming 525000, China

Corresponding author: Fei Zhang (zhangfei@dgut.edu.cn)

ABSTRACT Isogeometric analysis (IGA), due to its high efficiency and accuracy, can be replaced by the conventional finite element method in the topology optimizations (TOs). In this paper, we present an efficient isogeometric TO method based on the scheme of bi-directional evolutionary structural optimization (BESO). The structural response analysis is implemented by the IGA, and the detailed derivation is introduced. Based on the local support property of the non-uniform rational B-spline (NURBS), a NURBS filter is proposed to smooth the sensitivity numbers, of which NURBS space is different from that used in the IGA as long as the element spans keep consistency. Three benchmark numerical examples with different filters and mesh sizes are presented to validate the stability and mesh-dependency of the proposed isogeometric TO method.

INDEX TERMS Isogeometric analysis (IGA), topology optimization, bi-directional evolutionary structural optimization, NURBS filter.

I. INTRODUCTION

Topology optimization (TO) is one of the most effective approaches to find the optimal material distribution in a design domain in order to obtain the best structural performance. Since the pioneer work of Bendsoe and Kikuchi [1], TO has been widely used to solve the problems in mechanical [2] and many other engineering domains, such as fluids [3], acoustics [4], heat transfer [5], optics [6], multiphysics [7] and functional material design [8]–[10]. Many subsequent approaches have been proposed to solve TO problems in the past thirty years, such as homogenization method [1], solid isotropic material with penalization (SIMP) approach [11], [12], level set method [13]–[17], and evolutionary structural optimization (ESO) approach [18], [19]. Among these, the ESO method is one of the most popular TO approaches due to its simple concept of gradually removing

The associate editor coordinating the review of this manuscript and approving it for publication was Sotirios Goudos.

inefficient material from a structure. The ESO method was first proposed by Xie and Steven in the early 1990s [18]. The idea is based on an empirical concept that structure evolves towards an optimum by slowly removing elements with lowest stresses. Later, a new version of the ESO method, named the bi-directional evolutionary structural optimization (BESO), allows material to be removed and added simultaneously [19]. Recently, a extended BESO with smoothed boundary was proposed by Da *et al.* [20], where the smooth topology was determined by a level-set function. Compared with the ESO, the BESO is more stable and less dependent on the used parameters, and has been used for a wide range of applications including both macrostructures and microstructures [21]–[27], and more details can be found in a recent BESO review [28].

In general, the finite element method (FEM) [29] is used for the structural response analysis in the TO. However, using FEM in TO has to face some drawbacks caused by numerical problems of the FEM, e.g., the disconnection between

analysis models and geometric models, the low continuity between the elements, and the low efficiency for high-order elements [30] In recent years, isogeometric analysis (IGA) [31], [32], where the basis functions of the geometric model are directly used for structural analysis, has become one of the most efficient methods in a variety of domains [33]–[40]. Due to the advantages of IGA, e.g., high efficiency, high accuracy and high continuity, IGA has been also introduced to TO instead of the FEM to achieve better performance. For example, high-order elements that is able to relieve checkerboards [41], [42], [65] can be implemented in IGA without increasing as much computational cost as that in the FEM.

The first isogeometric TO was proposed by Seo *et al.* [43], where the trimmed surface analysis technique [44] was employed for the structural response analysis and the sensitivity, which was complicated and time-consuming. Kumar and Parthasarathy [45] used B-spline finite elements in density-based TO to obtain results that were free from checkerboard artifacts. Hassani *et al.* [46] proposed an isogeometric approach to TO in which the control point based SIMP method was employed and the physical fields were interpolated by Non-uniform rational B-spline (NURBS) basis functions. Dedè *et al.* [47] presented IGA for TO with a phase field model in both 2D and 3D problems, and demonstrated that IGA was particularly suitable for phase field problems and allowed exact CAD geometry in the TO. Different from the above work that focused on using IGA to replace FEM in TO, Qian [48] presented a density-based TO whose design space was restricted to the B-spline space, and the B-spline space was free from checkerboards without additional filtering, but the computation of the structural analysis and the sensitivity was still implemented by the conventional FEM. Moreover, there are several researchers combining IGA with level-set based TO, Wang and Benson [30], [49] proposed an isogeometric parameterized level set TO where the level set function was discretized using NURBS basis functions and the structural analysis was completed by IGA, and later extended it to solve geometric constrained problems. Xia *et al.* [50] proposed a GPU parallel isogeometric level set TO, and the speedups achieve two orders of magnitude. Wang *et al.* [51] presented an adaptive chaotic particle swarm algorithm for isogeometric multi-objective size optimization of functionally graded plates. Jahangiry and Tavakkoli [52] proposed applied IGA to level set TO and solved three optimization problems including minimization of the mean compliance considering a certain amount of materials, minimization of weight with avoiding local stress concentration as well as minimization of weight and strain energy under local stress constraints. Recently, IGA was also integrated into an explicit topology optimization based on moving morphable components (MMC), where the design variables were a set of geometric parameters such as coordinates of center, length, variable thicknesses and inclined angle [53], [54]. Besides, IGA was successfully used in multi-scale or multi-material TOs [55], [56]. More details about isogeometric topology

optimization can be found in a recent review [57]. However, although some researchers also tried to combine IGA and with BESO, such as the work in reference [58], the optimization details were unclear and the example analysis was vague.

In this paper, a NURBS-based isogeometric BESO framework is presented to achieve the optimal structure with minimum mean compliance. Apart from the structural analysis implemented by the IGA, a NURBS filter is proposed to replace the sensitivity filter of the conventional BESO, and the different filters are compared in detail. The organization of the rest of this paper is as follows. Section 2 briefly introduces the basic theory of the proposed optimization framework including the BESO and the fundamentals of IGA. Section 3 describes the isogeoemtric BESO for plane elasticity problems, as well as the NURBS filter and the numerical implementation. Thereafter benchmark problems are presented in Section 4 to demonstrate the efficiency and stability of the proposed TO method. Finally, conclusion and future research are discussed in Section 5.

II. BASIC THEORY
A. BI-DIRECTIONAL EVOLUTIONARY STRUCTURAL OPTIMIZATION
1) STATEMENT OF OPTIMIZATION PROBLEM
The bi-directional evolutionary structural optimization (BESO) method allows not only removing materials, but also adding materials. In the original BESO, the optimal topology is determined according to the relative ranking of the sensitivity numbers. It is difficult to estimate the sensitivity numbers of the void elements since no information available for the void elements which are not included in the finite element analysis. Therefore, a new version of BESO utilizing material interpolation scheme with penalization as that in SIMP was proposed by Huang and Xie [59], and our work is based on the new BESO. For the minimum compliance problem, the optimization problem can be stated as follows

$$\text{Minimize}: \ C = \frac{1}{2}\boldsymbol{u}^T\boldsymbol{K}\boldsymbol{u}$$
$$\text{subject to}: \ V^* - \sum_{i=1}^{N} V_i x_i = 0$$
$$x_i = x_{\min} \text{ or } 1 \tag{1}$$

where C is the mean compliance, $\boldsymbol{K}$ and $\boldsymbol{u}$ are the global stiffness matrix and the displacement vector, V_i is the volume of an individual element, V^* is the prescribed structural volume, ie., the volume fraction. N is the total number of elements, and the design variable x_i denotes the relative density of the ith element. It is noted that a small value of $x_{\min}$ (e.g., 0.001) is used to represent the density of a void element.

2) SENSITIVITY ANALYSIS
Using the material interpolation scheme of SIMP into BESO, Young's modulus of the intermediate material can be interpolated as

$$E(x_i) = x_i^{\beta} E_0, \tag{2}$$

where E_0 is the Young's modulus of the solid material and β is the penalty factor (typically $\beta = 3$).

Based on Equation (2), the sensitivity of the objective function C with respect to the element density x_i can be found as

$$\frac{\partial C}{\partial x_i} = -\frac{\beta x_i^{\beta-1}}{2} \boldsymbol{u}_i^T \boldsymbol{K}_i^0 \boldsymbol{u}_i, \tag{3}$$

where u_i is the element displacement vector, and K_i^0 is the element stiffness matrix for solid elements. In BESO, a structure is optimized using discrete design variables. Hence, only two materials are allowed in the design, and the element sensitivities for both solid and soft elements can be written as [59]

$$\alpha_i = -\frac{1}{\beta}\frac{\partial C}{\partial x_i} = \begin{cases} \frac{1}{2}\boldsymbol{u}_i^T \boldsymbol{K}_i^0 \boldsymbol{u}_i & \text{when } x_i = 1 \\ \frac{x_{\min}^{\beta-1}}{2}\boldsymbol{u}_i^T \boldsymbol{K}_i^0 \boldsymbol{u}_i & \text{when } x_i = x_{\min}, \end{cases} \tag{4}$$

where α_i is the sensitivity number of the ith element.

3) MESH-INDEPENDENT FILTER
To avoid numerical instabilities such as checkerboard and mesh-dependency, a filter technique is usually applied to smooth the sensitivity number. The BESO mesh-independency filter works similarly as the sensitivity filter in the SIMP method, which can be expressed by

$$\hat{\alpha}_i = \frac{1}{\sum_{j\in N_i} H_{ij}} \sum_{j\in N_i} H_{ij}\alpha_j, \tag{5}$$

where N_i is the set of elements j for which the center-to-center distance r_{ij} to element i is smaller than the filter radius r_{min} and H_{ij} is a weight factor defined as

$$H_{ij} = \max\left(0, r_{\min} - r_{ij}\right). \tag{6}$$

To improve the convergence, the sensitivity number can be averaged with its historical information [59], which is simply expressed by

$$\tilde{\alpha}_i = \frac{1}{2}(\hat{\alpha}_{i,k-1} + \hat{\alpha}_{i,k}), \tag{7}$$

where k is the current iteration number.

B. EVOLUTION PROCEDURE
In BESO, the topology gradually evolves by iterations, and the following equation is used to determine the structural volume of the next iteration.

$$V^{k+1} = \begin{cases} \max\left(V^k\left(1-ER\right), V^*\right) & \text{when } V^k > V^* \\ \min\left(V^k\left(1+ER\right), V^*\right) & \text{when } V^k \le V^*, \end{cases} \tag{8}$$

where V^* is the objective volume, V^k is the resultant volume of the kth iteration, V^{k+1} is the target volume for the next design (i.e., the next iteration), ER denotes the evolutionary rate that defines the maximum variation of the volume in one iteration.

The evolution will be stopped when the convergence criterion is satisfied, and the optimal structure is obtained.

The convergence criterion is defined as a function of the variation of the objective function as

$$\frac{\sum_{i=1}^{N}\left(C_{k-i+1} - C_{k-N-i+1}\right)}{\sum_{i=1}^{N} C_{k-i+1}} < \varepsilon, \tag{9}$$

where k is current iteration number, ε is a preset convergence error and N is an integer number which are set to 0.001 and 5 respectively in this work. It should be noted that there is at least 10 iterations when the integer N is set to 5 according to Equation (9).

C. SUMMARY OF NURBS
Non-uniform rational B-splines (NURBS), constructed from B-splines, are commonly used in computer-aided design (CAD) and computer graphics (CG) [60]. A knot vector $\Xi = \{\xi_1, \xi_2, \ldots, \xi_{n+p+1}\}$ is a sequence of non-decreasing real numbers in the parametric space, where n and p are the number of control points and the spline order respectively. The interval $[\xi_1, \xi_{n+p+1}]$ is a patch and the knot interval $[\xi_1, \xi_{i+1})$ is a span.

According to the Cox-de Boor recursion formula [61], the B-spline basis functions $B_{i,p}(\xi)$ can be defined as

$$B_{i,0}(\xi) = \begin{cases} 1, & if\, \xi_i \le \xi < \xi_{i+1} \\ 0, & otherwise, \end{cases}$$

$$B_{i,p}(\xi) = \frac{\xi - \xi_i}{\xi_{i+p} - \xi_i}B_{i,p-1}(\xi) + \frac{\xi_{i+p+1} - \xi}{\xi_{i+p+1} - \xi_{i+1}}$$
$$\times B_{i+1,p-1}(\xi),\, (p > 0), \tag{10}$$

where we define the convention $0/0 = 0$.

Dividing B-spline basis functions by a positive weight w_i, a NURBS basis function can be defined as

$$N_{i,p}(\xi) = \frac{B_{i,p}(\xi)w_i}{\sum_{j=1}^{n} B_{j,p}(\xi)w_j}. \tag{11}$$

There are four important properties of NURBS basis functions: (1) Nonnegativity: $N_{i,p}(\xi) \ge 0$; (2) Partition of unity: $\sum_{i=1}^{n} N_{i,p}(\xi) = 1$; (3) Local support: $N_{i,p}(\xi) = 0$ for $\xi \notin [\xi_i, \xi_{i+p+1})$; and (4) Differentiability: $N_{i,p}(\xi)$ is $p - k$ times differentiable where k is the multiplicity of the knots.

To represent a surface, two-dimensional NURBS basis functions of order p in ξ direction and order q in η direction are constructed as

$$N_{i,p}^{j,q}(\xi, \eta) = N_{i,p}(\xi)N_{j,q}(\eta), \tag{12}$$

and a NURBS surface is a bivariate piecewise rational function in the form of

$$S(\xi, \eta) = \sum_{i=1}^{n}\sum_{j=1}^{m} N_{i,p}^{j,q}(\xi, \eta)P_{i,j}, \tag{13}$$

where $P_{i,j}$ are the control points, and the patch for this surface is $[\xi_1, \xi_2, \ldots \xi_{n+p+1}] \times [\eta_1, \eta_2, \ldots \eta_{m+q+1}]$.

III. ISOGEOMETRIC BESO

A. ISOGEOMETRIC ANALYSIS

In the isogometric BESO, the isogeometric analysis (IGA) is used to replace FEM in the numerical computations of a given physical field. In NURBS-based IGA, the NURBS basis functions (e.g., Equations (11) and (13)) represent the CAD models which are directly used in structural analysis as shape functions. Hence, a variable x (e.g., coordinate, displacement, or force) whose parametric coordinate is (ξ, η) can be evaluated from the control point values

$$x(\xi, \eta) = \sum_i N_i(\xi, \eta)x_i, \qquad (14)$$

where N_i and x_i are the basis function and the variable value of the ith control point, respectively.

For the minimum compliance problem (a linear elasticity problem), the discrete equilibrium equation to be solved can be written as

$$Ku = F, \qquad (15)$$

in which K is the global stiffness matrix, u is the displacement vector and F is the external force vector associated with the control points. In terms of the NURBS interpolation, the elementary stiffness matrix K_e constructing the global stiffness matrix K can be written as

$$K_e = \int_{\Omega_e} B^T DB d\Omega = \int_{\bar{\Omega}_e} B^T DB |J_1||J_2|d\bar{\Omega}, \qquad (16)$$

where B is the strain-displacement matrix and D is the stress-strain matrix, Ω_e and $\bar{\Omega}_e$ are the physical and integration domains of the element. It should be noted that there are two Jacobians J_1 and J_2, which indicate the transformation relationship that map integrals from the NURBS parametric space to the physical space, and from the integration parametric space to the NURBS parametric space respectively.

For the sake of simplicity, we only consider 2D plane stress problems in this research work. Therefore, the stain-displacement matrix B is written as

$$B = \begin{bmatrix} \dfrac{\partial N_1}{\partial x} & 0 & \cdots & \dfrac{\partial N_n}{\partial x} & 0 \\ 0 & \dfrac{\partial N_1}{\partial y} & \cdots & 0 & \dfrac{\partial N_n}{\partial y} \\ \dfrac{\partial N_1}{\partial y} & \dfrac{\partial N_1}{\partial x} & \cdots & \dfrac{\partial N_n}{\partial y} & \dfrac{\partial N_n}{\partial x} \end{bmatrix}, \qquad (17)$$

and

$$\begin{bmatrix} \dfrac{\partial N_i}{\partial x} & \dfrac{\partial N_i}{\partial y} \end{bmatrix} = \begin{bmatrix} \dfrac{\partial N_i}{\partial \xi} & \dfrac{\partial N_i}{\partial \eta} \end{bmatrix} J_1^{-1}, \qquad (18)$$

where N_i is the ith basis function of the NURBS element, and the Jacobian J_1 is formulated as

$$J_1 = \begin{bmatrix} \dfrac{\partial x}{\partial \xi} & \dfrac{\partial y}{\partial \xi} \\ \dfrac{\partial x}{\partial \eta} & \dfrac{\partial y}{\partial \eta} \end{bmatrix}. \qquad (19)$$
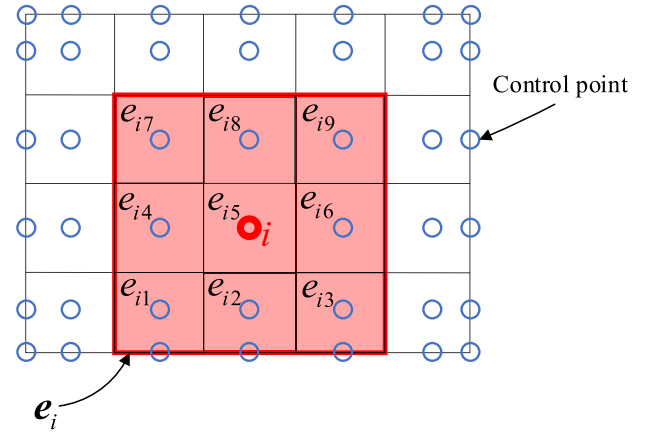

FIGURE 1. Illustration of the relation between a control point i and its corresponding elements.

For isotropic materials, the stress-strain matrix D may be written as

$$D = \frac{E}{1 - v^2} \begin{bmatrix} 1 & v & 0 \\ v & 1 & 0 \\ 0 & 0 & \dfrac{1-v}{2} \end{bmatrix}, \qquad (20)$$

where E is the Young's modulus and v is the Poisson's ratio. The Jacobian J_2 is expressed as

$$J_2 = \begin{bmatrix} \dfrac{\partial \xi}{\partial \bar{\xi}} & \dfrac{\partial \eta}{\partial \bar{\xi}} \\ \dfrac{\partial \xi}{\partial \bar{\eta}} & \dfrac{\partial \eta}{\partial \bar{\eta}} \end{bmatrix} = \begin{bmatrix} \dfrac{\xi_{i+1} - \xi_i}{2} & 0 \\ 0 & \dfrac{\eta_{j+1} - \eta_j}{2} \end{bmatrix}. \qquad (21)$$

where $(\bar{\xi}, \bar{\eta})$ are the parametric coordinates of the Gauss quadrature domain.

B. CONTROL-POINT BASED BESO

In the original BESO, the element-based sensitivity of the objective function C is calculated by Equation (3) and the corresponding sensitivity number α_i is calculated by Equation (4). When the IGA is used, the design variables should be changed from element densities to control point densities, and the sensitivity of a control point is written as

$$\frac{\partial C}{\partial \tilde{x}_i} = \sum_{j \in e_i} \frac{\partial C}{\partial x_{e_{ij}}} \frac{\partial x_{e_{ij}}}{\partial \tilde{x}_i} = \sum_{j \in e_i}$$
$$- \frac{\beta \left(x_{e_{ij}}\right)^{\beta-1}}{2} u_{e_{ij}}^T K_{e_{ij}}^0 u_{e_{ij}} \frac{\partial x_{e_{ij}}}{\partial \tilde{x}_i}. \qquad (22)$$

where $\tilde{x}_i$ denotes the variable (i.e., density) of the ith control point, e_i is the element set on which the ith control point influences, e_{ij} is the jth element of e_i. Figure 1 gives an illustration of a control point and its corresponding elements, which is based on a NURBS patch

$$[0, 0, 0, 0.2, 0.4, 0.6, 0.8, 1, 1, 1]$$
$$\times [0, 0, 0, 0.25, 0.5, 0.75, 1, 1, 1].$$

Since the density is constant in an element, an element density x_i is represented by the density at the element center $x(ic)$, which is calculated by

$$x_i = x(ic) = \sum_{j \in \boldsymbol{c}_i} N_{c_{ij}}(ic)\tilde{x}_{c_{ij}}, \qquad (23)$$

where ic denotes the center of the ith element, c_i is the control point set that influences element i, c_{ij} is the jth control point of c_i, and $N_{c_{ij}}(ic)$ is the NURBS basis function of control point c_{ij} corresponding to the center of element i. Figure 2 gives an illustration of an element and its corresponding control points, which is based on the same NURBS patch as that in Figure 1.
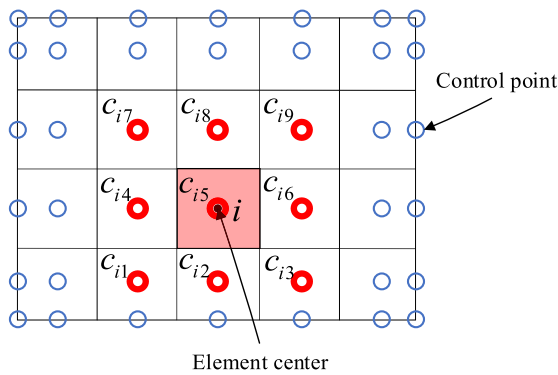
FIGURE 2. Illustration of the relation between an element i and its control points.

Based on Equation (23), the sensitivity of x_i with respect to a design variable $\tilde{x}_k$ is calculated by

$$\frac{\partial x_i}{\partial \tilde{x}_k} = N_k(ic), \qquad (24)$$

and thereby $\frac{\partial x_{e_{ij}}}{\partial \tilde{x}_i}$ in Equation (22) can be obtained according to the above equation.

When the sensitivities are obtained, the sensitivity number based on the NURBS control points can be written as

$$\tilde{\alpha}_i = -\frac{1}{\beta}\frac{\partial C}{\partial \tilde{x}_i} = \sum_{j \in e_i} \frac{(x_{e_{ij}})^{\beta-1}}{2}\boldsymbol{u}_{e_{ij}}^T\boldsymbol{K}_{e_{ij}}^0\boldsymbol{u}_{e_{ij}}N_i(e_{ij}c), \quad (25)$$

where e_i is the element set on which the ith control point influences, e_{ij} is the jth element of e_i, $x_{e_{ij}} = 1$ when element e_{ij} is a solid element and $x_{e_{ij}} = x_{\min}$ when element e_{ij} is a void element.
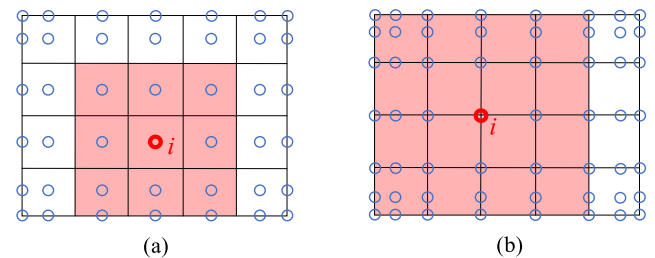
C. NURBS FILTER
In Section 2, a mesh-independent filter as Equation (5) is required to avoid numerical instabilities, where the weight factor H_{ij} is defined as a distance-based hat function that is in inverse proportion to the distance. In the BESO based on control points proposed, we do not need a distance-based hat function filter since the NURBS basis functions can replace this distance-based hat function, and such filter is called NURBS filter in this work. It shows the tensor product NURBS basis function corresponding to control point i,
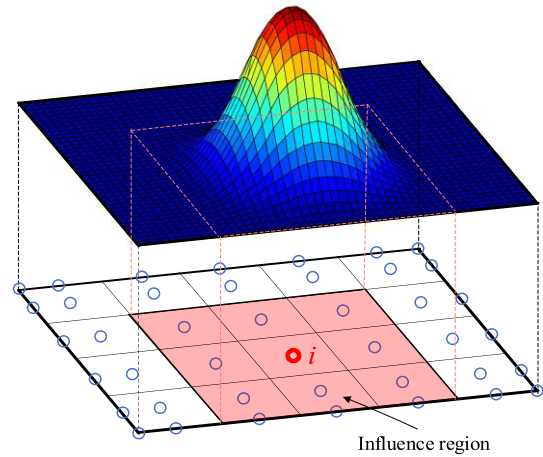
FIGURE 3. The tensor product NURBS basis function corresponding to control point i of Figure 1.

where we can find that the NURBS basis function is a natural distance-based hat function.

In Equation (25), the NURBS basis function works as a weight function, i.e., the sensitivity number is the spatial average of the adjacent NURBS basis functions, which corresponds to the weight function H_{ij} in Equation (5). The difference between NURBS filter and the conventional distance-based filter is that the NURBS basis function is piecewise polynomials of order $p \times q$, but the weight function H_{ij} is a linear distance function controlled by the filter radius r. Note that we do not need to define a filter radius for the NURBS filter with the help of the local support property of the NURBS basis function.

FIGURE 4. Influence region comparison of different NURBS orders p and q: (a) p = q = 2 and (b) p = q = 3.

Since no filter radius is defined in the NURBS filter, the influence region of a NURBS basis function is a rectangular region, e.g., the $(p+1) \times (q+1)$ knot spans, and Figure 4 shows an example of influence regions corresponding to different NURBS orders. In this work, we can use different p and q for IGA computation and NURBS filter as long as the NURBS spans keep constant. Therefore, we can only increase the order of the NURBS filter without changing the NURBS order of the IGA. It should be noted that the sensitivity numbers corresponding to the control points of the NURBS filter may be different from the control points of the IGA used in the structural response analysis.
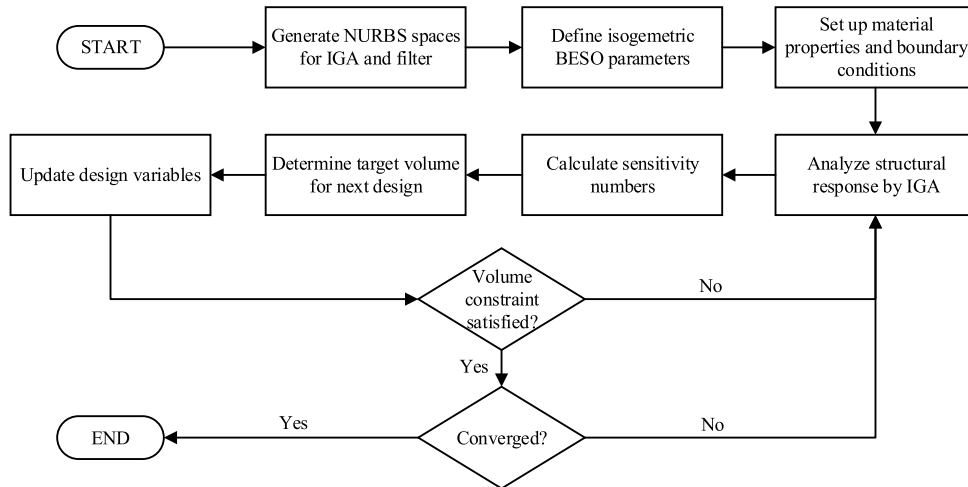
FIGURE 5. Flowchart of the isogeometric BESO procedure.

D. OPTIMIZATION PROCEDURE

The evolution procedure of the isogeometric BESO is similar to the conventional BESO, but the structural response analysis is implemented by the NURBS-based IGA, and the sensitivity numbers are based on the control points of the NURBS filter. It can be outlined as follows:

Step 1. Generate NURBS spaces NS_1 and NS_2 for IGA and NURBS filter respectively.

Step 2. Define isogeometric BESO parameters such as objective volume V^*, evolutionary ratio ER, and penalty exponent β.

Step 3. Set up materials properties such as Young's modulus E and Poisson's ratio v, and boundary conditions such as force and support.

Step 4. Analyze the structural response by IGA based on NS_1 (Section 3.1).

Step 5. Calculate the sensitivity numbers of control points in NS_2 (Equation (25)).

Step 6. Determine the target volume for the next design, which is calculated by Equation (8). Here the volume is calculated by $\sum_{i=1}^{n} \tilde{V}_i \tilde{x}_i$ where $\tilde{V}_i$ and $\tilde{x}_i$ are the equivalent volume (the equivalent volumes of all control points are equal in this work) and density of the ith control point of NS_2.

Step 7. Update the design variables, i.e., the densities of control points of NS_2. The control point density is set to 1 and $x_{\min}$ for "solid" control points and "void" control points, respectively, which can be determined by the target material volume and ranking of the sensitivity number. After the new control point densities are obtained, Equation (23) is used to calculate the new element densities.

Step 8. Repeat Steps 4-7 until the objective volume V^* and the convergence criterion (Equation (9)) are satisfied.

Figure 5 shows the flowchart corresponding to the above procedure. It should be noted that the element densities (not the control point densities) are used in IGA to calculate the stiffness matrix in this work, and the element densities are calculated based on Equation (23).

IV. NUMERICAL EXAMPLES

Three benchmark examples for minimum compliance design are examined in this section with the goal of demonstrating the advantages of the proposed isogeometric BESO scheme. All examples are run on a laptop computer with CPU Intel Core i5-6200U of 2.40 GHz, RAM of 8 GB, and software MATLAB (Natick, Massachusetts, U.S.A). The Young's modulus for the solid material is 1.0 and the Poisson's ratio is 0.3. A Gauss quadrature rule of 3×3 is used for quadratic isogeometric elements. The evolutionary ratio ER is set to 0.2, penalty exponent β is set to 3, and the convergence criterion as Equation (9) is set to 0.001.
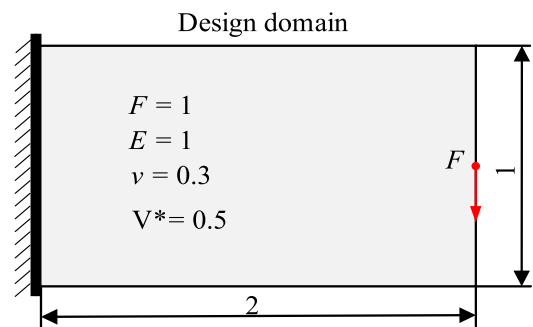

FIGURE 6. The design domain and parameter setting of the cantilever beam.

A. CANTILEVER BEAM

The cantilever beam problem is one of the most widely used TO benchmark problems [62], [63]. As shown in Figure 6, the cantilever beam is fixed on the left-hand side and loaded with a vertical point force at the center of the right-hand side. The design domain is discretized by a mesh of 80×40 quadratic NURBS elements (i.e. NURBS orders $p = q = 2$ for the IGA), and the volume fraction is set to 0.5, i.e. the result volume should be 50% of the

TABLE 1. Compliance and number of iterations for the TOs corresponding to Figure 7.

	NURBS filter $(p, q = 2)$	SIMP filter $(r = 1.5el)$	NURBS filter $(p, q = 3)$	SIMP filter $(r = 2.5el)$	NURBS filter $(p, q = 4)$	SIMP filter $(r = 3.5el)$
Compliance	32.13	32.31	31.97	32.01	31.38	33.88
Number of iterations	53	56	60	38	71	99

volume of design domain. Three different NURBS filters with $p = q = 2$, $p = q = 3$ and $p = q = 4$ are used separately to demonstrate effectiveness of the NURBS filter, which are also compared with the distance-based filters with filter radii $r = 1.5el$, $r = 2.5el$ and $r = 3.5el$ (el is the length of an element edge and such filtering region can be regarded as approximate equivalent to that of the abovementioned NURBS filters). Since the filtering region of NURBS filter is rectangle while that of SIMP filter is circular, it is approximate but not total equivalent for the filtering region of NURBS filter and SIMP filter with corresponding parameters. Since the distance-based filter is usually used in the SIMP method, we call it SIMP filter for short herein. Besides, the design variables are the element densities in the SIMP filter one, which is the same as the SIMP topology optimization.
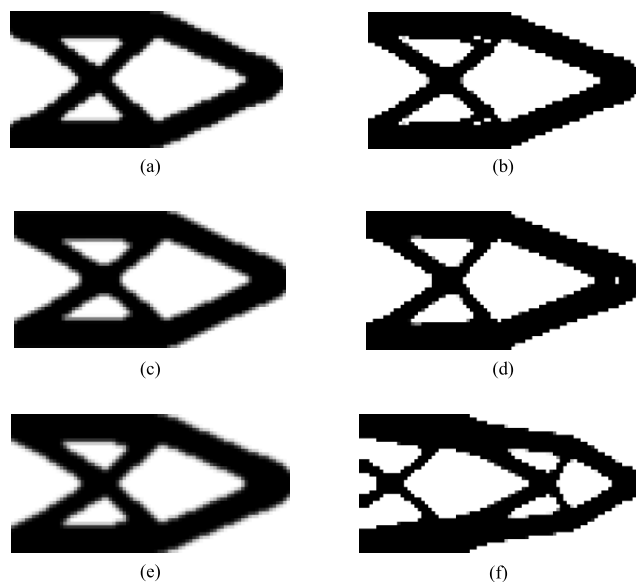

(a)

(b)

(c)

(d)

(e)

(f)

FIGURE 7. The optimization results of the cantilever beam: (a) NURBS filter with $p = q = 2$, (b) SIMP filter with $r = 1.5el$, (c) NURBS filter with $p = q = 3$, (d) SIMP filter with $r = 2.5el$, (e) NURBS filter with $p = q = 4$, and (f) SIMP filter with $r = 3.5el$.

Figure 7 shows the optimization results of the cantilever beam. From Figures 7(a), (c) and (e), it can be found that the optimization results of the NURBS filters with different influence regions are very similar, which demonstrates

$V^* = 0.5$
$R_{out} = 2$
$R_{in} = 1$
$F = 1$
$E = 1$
$v = 0.3$
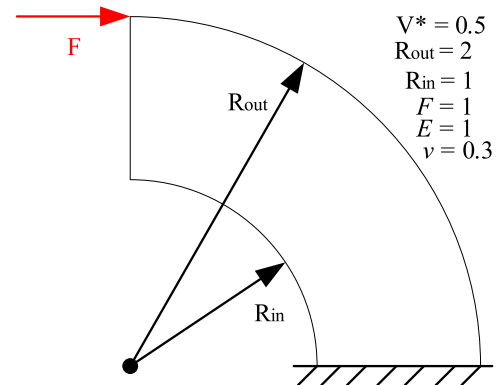
FIGURE 8. The design domain and parameters of quarter annulus structure.

the stability of the NURBS filters proposed in this work. From Figures 7(b), (d) and (f), it is easy to find that the final optimized structures are a little different between each other, especially for the result of Figure 7(f). The reason for this is that different filter radii influence the results of the optimization, but the NURBS filter is more stable than the SIMP filter in isogeomtric BESO. The optimization is more sensitive in the isogeomtric BESO with SIMP filters caused by the unmatched regions of control point and filter (i.e., the influence region of a control point is rectangular but the filtering region of SIMP filter is circular). Therefore, we have to manually choose a suitable filter radius to obtain the optimal result if SIMP filter is adopted, and this can be avoid by using the NURBS filter. Another thing can be observed is that there are some grey elements in Figures 7(a), (c) and (e). The major reason for this is that the design variables of the isogeomtric BESO with NURBS filters depend on the control points, but the visualization of the results are based on the elements, and the interpolation between the control point densities and the element densities as Equation (23) will result in medium densities, i.e., the grey elements. The grey elements can be avoided if we could design a new visualization method based on the control points. In isogeomtric BESO with SIMP filters, although the structural response analysis is implemented by IGA, the design variables still depend on

| (a) 60×30 | (b) 80×40 | (c) 100×50 |
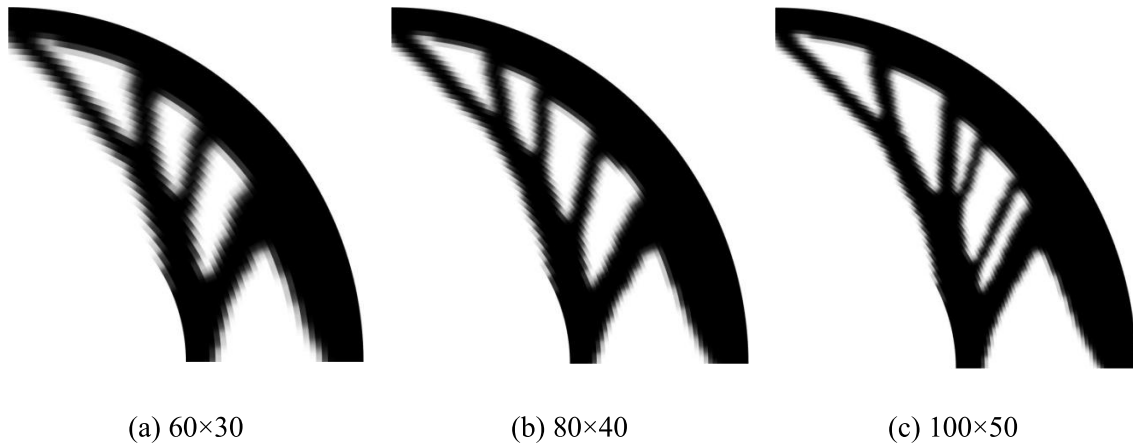
FIGURE 9. The final results of the quarter annulus structure: (a) mesh of 60 × 30 elements, (b) mesh of 80 × 40 elements, and (c) mesh of 100 × 50 elements.

the elements, so that almost only black elements are shown in Figure 7(b), (d) and (f). It should be noted that there are also very few grey elements in Figures 7(b), (d) and (f), which are caused by the modified sensitivity number as Equation (7), and the grey elements represent the difference between the final results and the results from the previous iteration.

Table 1 shows the compliance values and the number of iterations for the TOs shown in Figure 7. It can be found that the compliance becomes smaller when NURBS order increases in the isogeometric BESO with NURBS filters ($32.13 \rightarrow 31.97 \rightarrow 31.38$), and the convergence speed gradually decreases (number of iterations: $53 \rightarrow 60 \rightarrow 71$). For the SIMP-filter based method, the compliance decreases first and then increases, but the convergence speed increases first and then decreases. This further demonstrates the higher stability of the NURBS filters. It is noted that the compliance results obtained by NURBS filter method is lower than the SIMP filter method under the approximate filtering region, this is because the NURBS filter is similar to the IGA shape functions (i.e., NURBS basis functions), which makes it more suitable to obtain a lower-compliance result. In contrast, the distance-based SIMP filter is unmatched with the shape function. Therefore, it is recommended to use NURBS filters for the isogeometric BESO.

B. QUARTER ANNULUS STRUCTURE

To demonstrate that the isogeometric BESO can avoid spatial discretization error, a quarter annulus example with curved boundaries is utilized as shown in Figure 8. A concentrated force is horizontally loaded at left-top corner while the bottom edge is fixed. The design domain is discretized with 60 × 30, 80 × 40 and 100 × 50 quadratic NURBS elements, respectively, and the NURBS filter (p = q = 2) is used.

The final optimized results of isogeometric BESO with NURBS filter method based on different mesh sizes are presented in Figure 9. The perfect curved outer boundaries demonstrate that no spatial discretization error exists in isogeometric BESO. However, although IGA directly uses the

exact CAD model and no spatial discretization error exists, but the visualization here is based on the pixel mesh interpolated by the control points that will cause some boundaries looks non-smooth (the pixel mesh consists of curved elements). From Figure 9, it can be observed that more details are generated for the finer meshes. The reason for this is that the NURBS filters for these cases use the same order (i.e., $p = q = 2$) but the filtering regions are different due to the different mesh sizes. To avoid such mesh dependence, we should increase the orders of NURBS filters for the finer meshes to keep the filtering region unchanged, which is studied in the third benchmark problem.
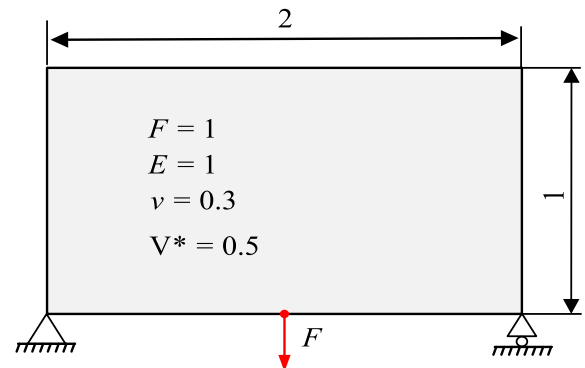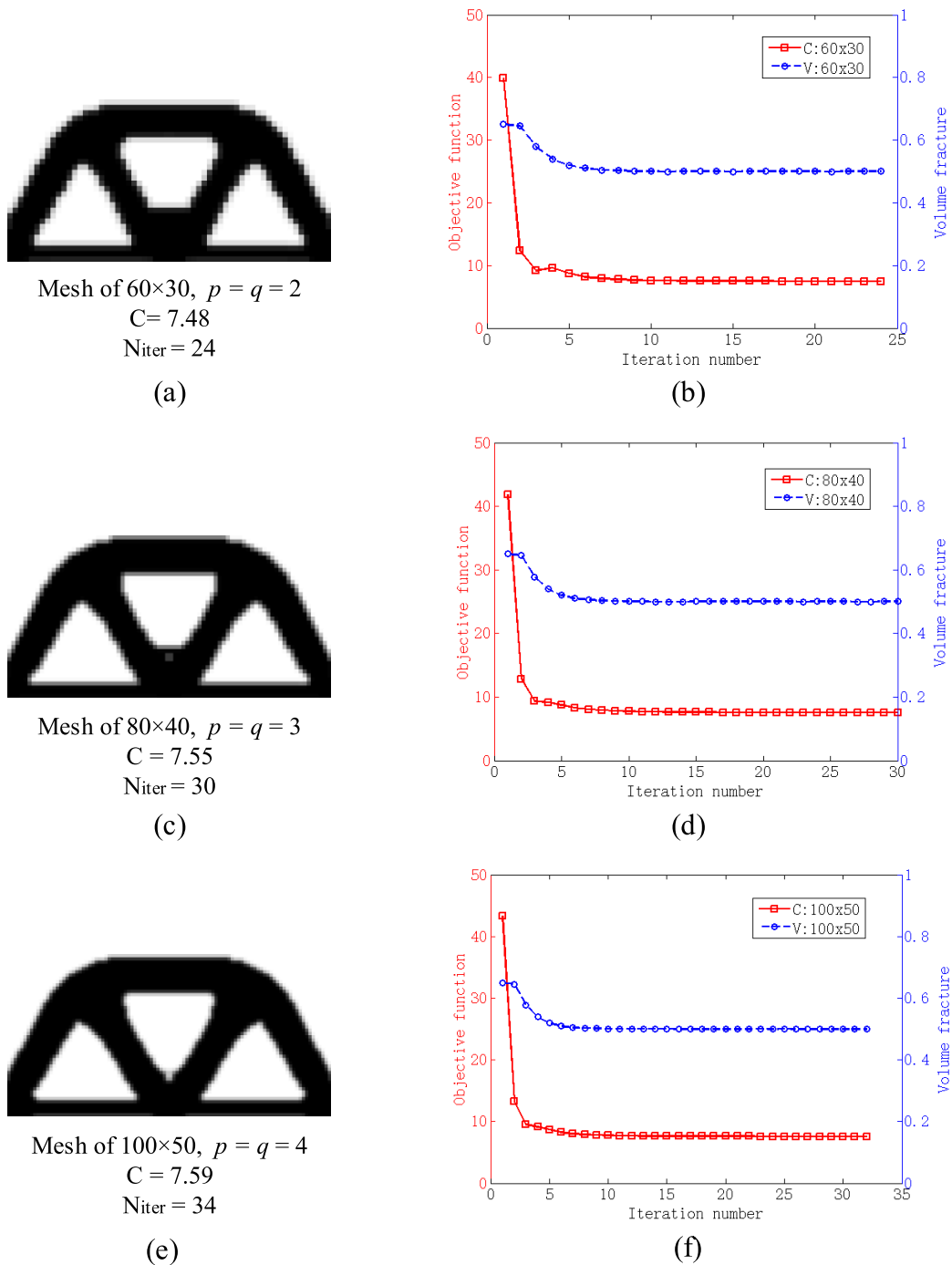

FIGURE 10. The design domain and parameters of Michell type structure.

C. MICHELL TYPE STRUCTURE

The third benchmark problem used to evaluate results of TOs is illustrated in Figure 10, which is commonly used to evaluate the merit of a TO method [18], [55]. A fixed constraint is applied at the bottom-left corner and a roller constraint at the bottom-right corner. In this example, we aim to compare the results of different mesh sizes. The design domain is discretized with 60 × 30, 80 × 40 and 100 × 50 quadratic NURBS elements, respectively, and the NURBS

Mesh of 60×30, $p = q = 2$
C= 7.48
N_{iter} = 24

(a)

(b)

Mesh of 80×40, $p = q = 3$
C = 7.55
N_{iter} = 30

(c)

(d)

Mesh of 100×50, $p = q = 4$
C = 7.59
N_{iter} = 34

(e)

(f)

FIGURE 11. The optimization results and convergence history of the Michell type structure: (a) optimization result of 60 × 30 elements, (b) convergence history of 60 × 30 elements, (c) optimization result of 80 × 40 elements, (d) convergence history of 80 × 40 elements, (e) optimization result of 100 × 50 elements, and (f) convergence history of 100 × 50 elements.

filter method is used. In order to make the influence region of the NURBS filter equal for different mesh sizes, the NURBS orders of the filter are adopted $p = q = 2$, $p = q = 3$ and $p = q = 4$ corresponding to the above cases, respectively.

Figure 11 shows the optimization results and the convergence history over the iterations. Compared with

Figure 11(a), (c) and (e), it can be found that all the optimized structures are consistent, eliminating the mesh dependence, which demonstrates the validity of the mesh-independent NURBS filter. The number of iterations increases with the growth of the number of elements, and the reason for this is that more elements with more degrees of freedom (DOFs)
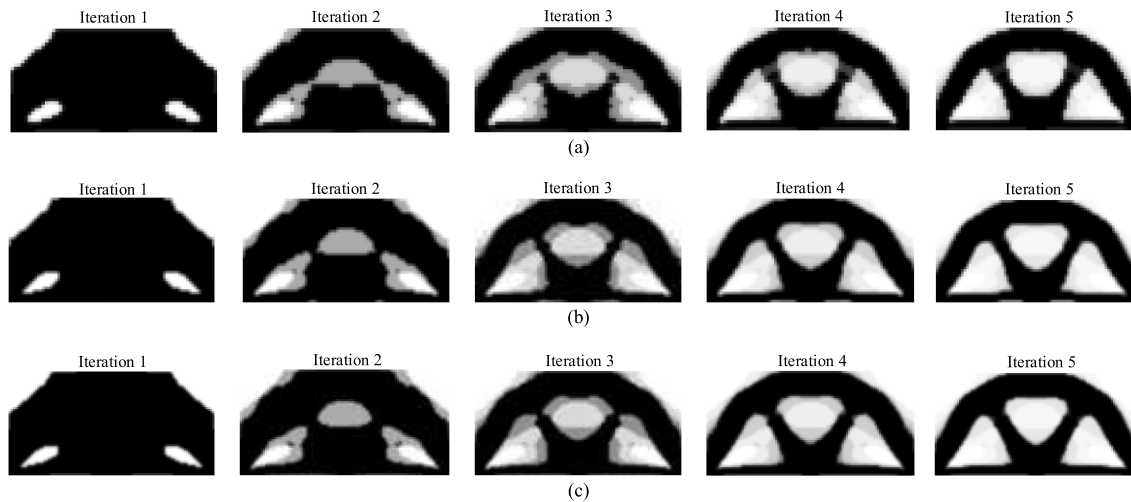
FIGURE 12. The results of the Michell type structure in the first five iterations: (a) mesh of 60 × 30 elements, (b) mesh of 80 × 40 elements, and (c) mesh of 100 × 50 elements.

need more iterations to achieve the convergence criterion. In numerical computation, more elements are able to obtain a more accurate result, and for the Michell type structure subjected to a concentrated force, the maximum stress will increase when finer elements are used. Therefore, the mean compliance value gradually increases with the element increasing (7.48 → 7.55 → 7.59). It should be noted that mean compliance will be almost the same when the element size is small enough, as the computational accuracy of IGA is high enough with such small element size.

From Figures 11(b), (d) and (f), It can be found that there is a small oscillation in the objective function curve before the 5th iteration, especially for the curve of Figure 11(b). The reason for this is that the structural topology changes very fast in the first 5 iterations (as shown in Figure 12) and the volume fraction gradually achieve the objective volume fracture, which may cause the convergence oscillation as that between the 3th and the 4th iterations, i.e., the objective function value of the 3th iteration is a little smaller than that of the 4th iteration. After the 5 iterations, the major structure has been obtained, and all left the iterations (19, 25 and 29 iterations for 60 × 30, 80 × 40 and 100 × 50 cases respectively) work on modifying the detail structure until the optimal structure is obtained. Comparing the optimization results of the 5th iteration in Figure 12 to the final optimal results in Figure 11, we can observe that they are similar, which means we only need several iterations to obtain a coarse but instructive optimization result without using too much time to implement the whole optimization procedure. Therefore, for a complex engineering optimization problem, we can only implement the initial iterations to evaluate the result first, and then make some necessary modification in terms of the coarse result before implementing a complete optimization, which will improve the efficiency.

V. CONCLUSION

This paper presented an isogeometric TO based on the BESO scheme for minimum compliance problems. In the proposed method, sensitivity numbers are calculated based on the NUBRS control points, and the structural response analysis is implemented by the isogeometric analysis (IGA) which directly uses exact geometry in the analysis and avoids the spatial discretization error of the conventional FEM. Besides, a NURBS filter whose NURBS space may be different from that used in the IGA. By changing the spline order of the NURBS filter, we can change the influence region of the filter. Three benchmark examples were tested in this work to verify the isogeometric TO method. In the cantilever beam example, we compared difference between the NURBS filter and the distance-based SIMP filter by modifying the influence region of the filters, and proved that the proposed NURBS filter is more stable and suitable for the isogeometric TO. In the Michell type structure, we further demonstrated the validity of the NURBS filter by different meshes and analyzed the convergence history of the isogeometric TO. By comparing with the topology evolution in detail, we concluded that the structural topology majorly changed in the initial iterations, most of the iterations were spent in the details improvement. In the quarter annulus structure, we demonstrated that no discretization error exists in isogeometric BESO, and further discussed the mesh dependence phenomenon of the NURBS filter. While the current work focuses on the minimum compliance problems only, further work will expand the proposed method to other fields, as well as the extension to more complex engineering problems [64].

A. DECLARATION OF CONFLICTING INTERESTS

The authors declared no potential conflicts of interest with respect to the research, authorship, and/or publication of this article.

B. DATA AVAILABLE STATEMENT

ACKNOWLEDGEMENT

REFERENCES

[1] M. P. Bendsøe and N. Kikuchi, "Generating optimal topologies in structural design using a homogenization method," *Comput. Method Appl. Mech. Eng.*, vol. 71, no. 2, pp. 197–224, Nov. 1988.

[2] O. Sigmund, "On the design of compliant mechanisms using topology optimization," *J. Struct. Mech.*, vol. 25, pp. 493–524, Apr. 1997.

[3] T. Borrvall and J. Petersson, "Topology optimization of fluids in Stokes flow," *Int. J. Numer. Methods Fluids*, vol. 41, pp. 77–107, Sep. 2003.

[4] E. Wadbro and M. Berggren, "Topology optimization of an acoustic horn," *Comput. methods Appl. Mech. Eng.*, vol. 196, pp. 420–436, Dec. 2006.

[5] A. Gersborg-Hansen, M. P. Bendsøe, and O. Sigmund, "Topology optimization of heat conduction problems using the finite volume method," *Struct. Multidisciplinary Optim.*, vol. 31, pp. 251–259, Apr. 2006.

[6] M. Zhou, B. S. Lazarov, and O. Sigmund, "Topology optimization for optical microlithography with partially coherent illumination," *Int. J. Numer. Methods Eng.*, vol. 109, pp. 631–647, May 2017.

[7] G. H. Yoon, "Topological layout design of electro-fluid-thermal-compliant actuator," *Comput. Methods Appl. Mech. Eng.*, vol. 209, pp. 28–44, Feb. 2012.

[8] J. K. Guest and J. H. Prévost, "Design of maximum permeability material structures," *Comput. Methods Appl. Mech. Eng.*, vol. 196, pp. 1006–1017, Jan. 2007.

[9] Y. Chen, S. Zhou, and Q. Li, "Computational design for multifunctional microstructural composites," *Int. J. Mod. Phys. B*, vol. 23, pp. 1345–1351, 2009.

[10] L. Xia and P. Breitkopf, "Design of materials using topology optimization and energy-based homogenization approach in MATLAB," *Struct. Multidisciplinary Optim.*, vol. 52, pp. 1229–1241, Jul. 2015.

[11] M. P. Bendsøe, "Optimal shape design as a material distribution problem," *Struct. Optim.*, vol. 1, no. 4, pp. 193–202, Dec. 1989.

[12] M. Zhou and G. I. N. Rozvany, "The COC algorithm, Part II: Topological, geometrical and generalized shape optimization," *Comput. Methods Appl. Mech. Eng.*, vol. 89, pp. 309–336, Feb. 1991.

[13] G. Allaire, F. Jouve, and A. M. Toader, "Structural optimization using sensitivity analysis and a level-set method," *J. Comput. Phys.*, vol. 194, pp. 363–393, Feb. 2004.

[14] M. Yulin and W. Xiaoming, "A level set method for structural topology optimization and its applications," *Comput. Methods Appl. Mech. Eng.*, vol. 35, pp. 415–441, Jul. 2004.

[15] Q. Xia, M. Y. Wang, and T. Shi, "A level set method for shape and topology optimization of both structure and support of continuum structures," *Comput. Methods Appl. Mech. Eng.*, vol. 272, pp. 340–353, Apr. 2014.

[16] T. Liu, B. Li, S. Wang, and L. Gao, "Eigenvalue topology optimization of structures using a parameterized level set method," *Struct. Multidisciplinary Optim.*, vol. 50, pp. 573–591, Oct. 2014.

[17] R. Li and B. Zhu, "An augmented formulation of distributed compliant mechanism optimization using a level set method," *Adv. Mech. Eng.*, vol. 8, pp. 1–10, Aug. 2016.

[18] Y. M. Xie and G. P. Steven, "A simple evolutionary procedure for structural optimization," *Comput. Struct.*, vol. 49, pp. 885–896, Dec. 1993.

[19] O. M. Querin, G. P. Steven, and Y. M. Xie, "Evolutionary structural optimisation (ESO) using a bidirectional algorithm," *Eng. Comput.*, vol. 15, no. 8, pp. 1031–1048, 1998.

[20] D. Da, L. Xia, G. Li, and X. Huang, "Evolutionary topology optimization of continuum structures with smooth boundary representation," *Struct. Multidisciplinary Optim.*, vol. 57, pp. 2143–2159, Jun. 2018.

[21] X. Huang and Y. M. Xie, *Evolutionary Topology Optimization of Continuum Structures: Methods and Applications*. Hoboken, NJ, USA: Wiley, 2010.

[22] X. Huang and Y.-M. Xie, "A further review of ESO type methods for topology optimization," *Struct. Multidisciplinary Optim.*, vol. 41, pp. 671–683, May 2010.

[23] B. Xu, H. Ding, and Y. M. Xie, "Optimal design of material microstructure for maximizing damping dissipation velocity of piezoelectric composite beam," *Int. J. Mech. Sci.*, vols. 128–129, pp. 527–540, Aug. 2017.

[24] L. Xia, F. Fritzen, and P. Breitkopf, "Evolutionary topology optimization of elastoplastic structures," *Struct. Multidisciplinary Optim.*, vol. 55, pp. 569–581, Feb. 2017.

[25] K. Li, Y. Wang, Y. Lin, W. Xu, and M. Liu, "A novel two-stage optimization method for beam–plate structure design," *Adv. Mech. Eng.*, vol. 8, pp. 1–18, Nov. 2016.

[26] T. Tang, B. Li, X. Fu, Y. Xi, and G. Yang, "Bi-directional evolutionary topology optimization for designing a neutrally buoyant underwater glider," *Eng. Optim.*, vol. 50, pp. 1270–1286, Nov. 2018.

[27] N. Gan, S. Yao, Y. Xiong, and X. Hong, "A hybrid cellular automaton–bi-directional evolutionary optimization algorithm for topological optimization of crashworthiness," *Eng. Optim.*, vol. 50, pp. 2054–2070, Feb. 2018.

[28] L. Xia, Q. Xia, X. Huang, and Y. M. Xie, "Bi-directional evolutionary structural optimization on advanced structures and materials: A comprehensive review," *Arch. Comput. Methods Eng.*, vol. 25, no. 2, pp. 437–478, Apr. 2018.

[29] T. J. R. Hughes, *The Finite Element Method: Linear Static and Dynamic Finite Element Analysis*. North Chelmsford, MA, USA: Courier Corporation, 2012.

[30] Y. Wang and D. J. Benson, "Isogeometric analysis for parameterized LSM-based structural topology optimization," *Comput. Mech.*, vol. 57, pp. 19–35, Jan. 2016.

[31] T. J. R. Hughes, J. A. Cottrell, and Y. Bazilevs, "Isogeometric analysis: CAD, finite elements, NURBS, exact geometry and mesh refinement," *Comput. Methods Appl. Mech. Eng.*, vol. 194, nos. 39–41, pp. 4135–4195, Oct. 2005.

[32] J. A. Cottrell, T. J. R. Hughes, and Y. Bazilevs, *Isogeometric Analysis: Toward Integration of CAD and FEA*. Hoboken, NJ, USA: Wiley, 2009.

[33] J. Yan, A. Korobenko, X. Deng, and Y. Bazilevs, "Computational free-surface fluid–structure interaction with application to floating offshore wind turbines," *Comput. Fluids*, vol. 141, pp. 155–174, Dec. 2016.

[34] Y. Bazilevs, X. Deng, A. Korobenko, F. L. di Scalea, M. D. Todd, and S. G. Taylor, "Isogeometric fatigue damage prediction in large-scale composite structures driven by dynamic sensor data," *J. Appl. Mech.*, vol. 82, Sep. 2015, Art. no. 091008.

[35] X. Deng, A. Korobenko, J. Yan, and Y. Bazilevs, "Isogeometric analysis of continuum damage in rotation-free composite shells," *Comput. Methods Appl. Mech. Eng.*, vol. 284, pp. 349–372, Feb. 2015.

[36] Y. Wang, D. J. Benson, and A. P. Nagy, "A multi-patch nonsingular isogeometric boundary element method using trimmed elements," *Comput. Mech.*, vol. 56, pp. 173–191, Jul. 2015.

[37] Y. J. Wang and D. J. Benson, "Multi-patch nonsingular isogeometric boundary element analysis in 3D," *Comput. Methods Appl. Mech. Eng.*, vol. 293, pp. 71–91, Apr. 2015.

[38] M.-C. Hsu, D. Kamensky, Y. Bazilevs, M. S. Sacks, and T. J. R. Hughes, "Fluid–structure interaction analysis of bioprosthetic heart valves: Significance of arterial wall deformation," *Comput. Mech.*, vol. 54, pp. 1055–1071, Oct. 2014.

[39] D. Schillinger, L. Dedè, M. A. Scott, J. A. Evans, M. J. Borden, and E. Rank, "An isogeometric design-through-analysis methodology based on adaptive hierarchical refinement of NURBS, immersed boundary methods, and T-spline CAD surfaces," *Comput. Methods Appl. Mech. Eng.*, vol. 249, pp. 116–150, Dec. 2012.

[40] T. Yu, J. Zhang, H. Hu, and T. Q. Bui, "A novel size-dependent quasi-3D isogeometric beam model for two-directional FG microbeams analysis," *Compos. Struct.*, vol. 211, pp. 76–88, Mar. 2019.

[41] A. Díaz and O. Sigmund, "Checkerboard patterns in layout optimization," *Struct. Optim.*, vol. 10, no. 1, pp. 40–45, Aug. 1995.

[42] O. Sigmund and K. Maute, "Topology optimization approaches," *Struct. Multidisciplinary Optim.*, vol. 48, no. 6, pp. 1031–1055, Dec. 2013.

[43] Y.-D. Seo, H.-J. Kim, and S.-K. Youn, "Isogeometric topology optimization using trimmed spline surfaces," *Comput. Methods Appl. Mech. Eng.*, vol. 199, nos. 49–52, pp. 3270–3296, Dec. 2010.

[44] H.-J. Kim, Y.-D. Seo, and S.-K. Youn, "Isogeometric analysis for trimmed CAD surfaces," *Comput. Methods Appl. Mech. Eng.*, vol. 198, nos. 37–40, pp. 2982–2995, Aug. 2009.

[45] A. V. Kumar and A. Parthasarathy, "Topology optimization using *B*-spline finite elements," *Struct. Multidisciplinary Optim.*, vol. 44, p. 471, Oct. 2011.

[46] B. Hassani, M. Khanzadi, and S. M. Tavakkoli, "An isogeometrical approach to structural topology optimization by optimality criteria," *Struct. Multidisciplinary Optim.*, vol. 45, no. 2, pp. 223–233, Feb. 2012.

[47] L. Dedé, M. J. Borden, and T. J. R. Hughes, "Isogeometric analysis for topology optimization with a phase field model," *Arch. Comput. Methods Eng.*, vol. 19, no. 3, pp. 427–465, Sep. 2012.

[48] X. Qian, "Topology optimization in B-spline space," *Comput. Methods Appl. Mech. Eng.*, vol. 265, pp. 15–35, Oct. 2013.

[49] Y. Wang and D. J. Benson, "Geometrically constrained isogeometric parameterized level-set based topology optimization via trimmed elements," *Frontiers Mech. Eng.*, vol. 11, no. 4, pp. 328–343, Dec. 2016.

[50] Z. Xia, Y. Wang, Q. Wang, and C. Mei, "GPU parallel strategy for parameterized LSM-based topology optimization using isogeometric analysis," *Struct. Multidisciplinary Optim.*, vol. 56, no. 2, pp. 413–434, Aug. 2017.

[51] C. Wang, T. Yu, J. L. Curiel-Sosa, N. Xie, and T. Q. Bui, "Adaptive chaotic particle swarm algorithm for isogeometric multi-objective size optimization of FG plates," *Struct. Multidisciplinary Optim.*, vol. 60, no. 2, pp. 757–778, Aug. 2019.

[52] H. A. Jahangiry and S. M. Tavakkoli, "An isogeometrical approach to structural level set topology optimization," *Comput. Methods Appl. Mech. Eng.*, vol. 319, pp. 240–257, Jun. 2017.

[53] W. Hou, Y. Gai, X. Zhu, X. Wang, C. Zhao, L. Xu, K. Jiang, and P. Hu, "Explicit isogeometric topology optimization using moving morphable components," *Comput. Methods Appl. Mech. Eng.*, vol. 326, pp. 694–712, Nov. 2017.

[54] X. Xie, S. Wang, M. Xu, and Y. Wang, "A new isogeometric topology optimization using moving morphable components based on R-functions and collocation schemes," *Comput. Methods Appl. Mech. Eng.*, vol. 339, pp. 61–90, Sep. 2018.

[55] Y. Wang, H. Xu, and D. Pasini, "Multiscale isogeometric topology optimization for lattice materials," *Comput. Methods Appl. Mech. Eng.*, vol. 316, pp. 568–585, Apr. 2017.

[56] A. H. Taheri and K. Suresh, "An isogeometric approach to topology optimization of multi-material and functionally graded structures," *Int. J. Numer. Methods Eng.*, vol. 109, no. 5, pp. 668–696, Feb. 2017.

[57] Y. Wang, Z.-P. Wang, Z. Xia, and L. H. Poh, "Structural design optimization using isogeometric analysis: A comprehensive review," *Comput. Model. Eng. Sci.*, vol. 117, pp. 455–507, Jan. 2018.

[58] N. S. Sahithi, K. N. V. Chandrasekhar, and T. M. Rao, "Isogeometric topology optimization of continuum structures using evolutionary algorithms," *J. Experim. Appl. Mech.*, vol. 8, no. 3, pp. 8–18, 2017.

[59] X. Huang and Y. Xie, "Bi-directional evolutionary topology optimization of continuum structures with one or multiple materials," *Comput. Mech.*, vol. 43, pp. 393–401, Jun. 2009.

[60] P. Les and T. Wayne, *The NURBS Book*. Berlin, Germany: Springer-Verlag, 1997.

[61] C. de Boor, "On calculating with *B*-splines," *J. Approximation Theory*, vol. 6, no. 1, pp. 50–62, Jul. 1972.

[62] O. Sigmund, "A 99 line topology optimization code written in MATLAB," *Struct. Multidisciplinary Optim.*, vol. 21, no. 2, pp. 120–127, Apr. 2001.

[63] E. Andreassen, A. Clausen, M. Schevenels, B. S. Lazarov, and O. Sigmund, "Efficient topology optimization in MATLAB using 88 lines of code," *Struct. Multidisciplinary Optim.*, vol. 43, no. 1, pp. 1–16, Jan. 2011.

[64] Y. Wang, S. Arabnejad, M. Tanzer, and D. Pasini, "Hip implant design with three-dimensional porous architecture of optimized graded density," *J. Mech. Des.*, vol. 140, no. 11, Aug. 2018, Art. no. 111406.

[65] L. Jianyu, S. Zhenzhong, P. M. Pardalos, H. Ying, Z. Shaohui, and L. Chuan, "A hybrid multi-objective genetic local search algorithm for the prize-collecting vehicle routing problem," *Inf. Sci.*, vol. 478, pp. 40–61, Apr. 2019.
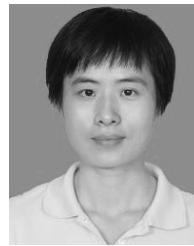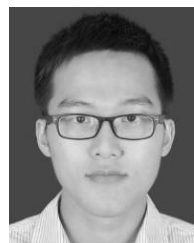
LING YIN received the Ph.D. degree in mechanical engineering from the Huazhong University of Science and Technology, Wuhan, China, in 2011. She started her career as an Associate Professor with the Dongguan University of Technology. Her research interests include digital design, intelligent manufacturing, and deep learning.

FEI ZHANG received the Ph.D. degree in mechanical engineering from the Huazhong University of Science and Technology, Wuhan, China, in 2017. He started his career as a Lecturer with the Dongguan University of Technology. His research interests include digital design and industry 4.0.

XIAOWEI DENG received the Ph.D. degree in aerospace engineering from the California Institute of Technology, in 2012. After then, he was with the University of California at San Diego, San Diego, CA, USA, as a Postdoctoral Fellow. In 2016, he started his career as an Assistant Professor with The University of Hong Kong.

PENG WU received the B.E. degree in mechanical engineering from the Dongguan University of Technology, Dongguan, China. He is currently pursuing the M.E. degree with Harbin Industrial University. He started his career with the Dongguan University of Technology. His research interests include mechanical design and artificial intelligence.

HONGXIN ZENG received the Ph.D. degree in industrial engineering from the Huazhong University of Science and Technology, Wuhan, China, in 2011. He is currently in project cooperated with the Hunan Provincial Key Laboratory of Health Maintenance for Mechanical Equipment, China. He started his career as an Associate Professor with the Dongguan University of Technology.

MEI LIU received the Ph.D. degree in control theory and control engineering from the South China University of Technology, Guangzhou, China, in 2010. She started her career as a Professor with the Guangdong University of Petrochemical Technology, Maoming, China. His research interests include sensing technology and system control.

• • •